



Natural Resources
Canada

Ressources naturelles
Canada

**GEOLOGICAL SURVEY OF CANADA
OPEN FILE 9168**

**Downhole geophysical logs in a shallow bedrock
aquifer near Fox Creek, Alberta**

H.L. Crow

2024

Canada

**GEOLOGICAL SURVEY OF CANADA
OPEN FILE 9168**

**Downhole geophysical logs in a shallow bedrock aquifer near
Fox Creek, Alberta**

H.L. Crow

2024

© His Majesty the King in Right of Canada, as represented by the Minister of Natural Resources, 2024

Information contained in this publication or product may be reproduced, in part or in whole, and by any means, for personal or public non-commercial purposes, without charge or further permission, unless otherwise specified.

You are asked to:

- exercise due diligence in ensuring the accuracy of the materials reproduced;
- indicate the complete title of the materials reproduced, and the name of the author organization; and
- indicate that the reproduction is a copy of an official work that is published by Natural Resources Canada (NRCan) and that the reproduction has not been produced in affiliation with, or with the endorsement of, NRCan.

Commercial reproduction and distribution is prohibited except with written permission from NRCan. For more information, contact NRCan at copyright-droitdauteur@nrcan-rncan.gc.ca.

Permanent link: <https://doi.org/10.4095/pzp3j11pfs>

This publication is available for free download through the NRCan Open Science and Technology Repository (<https://ostrnrcan-dostrncan.canada.ca/>).

Recommended citation

Crow, H.L., 2024. Downhole geophysical logs in a shallow bedrock aquifer near Fox Creek, Alberta; Geological Survey of Canada, Open File 9168, 1 .zip file. <https://doi.org/10.4095/pzp3j11pfs>

Publications in this series have not been edited; they are released as submitted by the author.

ISSN 2816-7155
ISBN 978-0-660-70451-7
Catalogue No. M183-2/9168E-PDF

Abstract

The Geological Survey of Canada (GSC) is investigating the vulnerability of shallow aquifers to oil and gas development activities near Fox Creek, AB. To support the project and provide input for hydrogeological models, downhole geophysical logs were collected in September 2020 in eight GSC-drilled observation wells (50 to 90 m in depth) to better understand the in situ lithological, geomechanical, and hydrogeological properties of the near-surface bedrock. The suite of logs included natural gamma and gamma-gamma density, camera and acoustic televiewer imagery, sonic logs to compute compressional (P-) and shear (S-) wave velocities, and fluid logs (temperature, conductivity, flow). Logs are interpreted alongside cuttings descriptions of the rock types. The roughness of the borehole walls presented some challenges in the interpretation of sonic logs, therefore results are compared to ultrasonic tests from two cores drilled adjacent to the logged wells. Velocities and densities are summarized by rock type, and geomechanical moduli (dynamic Poisson's ratio and Young modulus) are computed for the shallow bedrock. Hydrogeophysical logs indicate fluid is flowing both along fractures and through the sandstone rock matrix, and that groundwater recharge conditions (down flow) are prevalent across the site. Groundwater temperatures ranged between 3°C and 5°C, likely reflecting the mean annual air temperature. This report summarizes the downhole geophysical data acquisition and analyses, and provides log suites and digital data in appendices.

Contents

Abstract	i
Introduction.....	1
Geological and Hydrogeological Context.....	1
Borehole Drilling Program	2
Data Acquisition - Geophysical Logging	3
Data Processing and Analyses	5
Calibration.....	5
Processing	5
Acoustic Televiwer and 360° caliper	5
Full waveform sonic logs (P- and S-wave velocities)	8
Calculated Mechanical Properties.....	13
Flow meter data.....	13
Interpretation.....	14
Lithological Observations.....	14
Preliminary Structural Observations.....	17
Geomechanical Properties	18
Velocity and Density ranges by rock type	18
Elastic Moduli.....	18
Hydrogeophysical Logs	21
Vertical Fluid Flow	21
Fluid Properties	21
Fluid Pathways.....	24
Summary	27
Acknowledgements.....	28
References.....	29

Introduction

The Geological Survey of Canada (GSC) is characterizing the regional bedrock aquifer and investigating potential upward fluid migration pathways from deep oil and gas development activities to shallow aquifers in the area of Fox Creek, Alberta (Rivard et al., 2022). This area was selected because it has been one of the most active regions for oil and gas production in Canada over the past 50 years. To support the project's near surface aquifer assessment, downhole geophysical logs were acquired in eight GSC-drilled observation wells ranging in depth from 50 to 90 m. The suite of logs included:

- Nuclear logs (natural gamma and gamma-gamma density) to identify lithological variations along the boreholes and measure bulk rock density;
- Camera recordings to image conditions of the borehole walls and the movement of groundwater in the wells;
- Acoustic televiewer imagery to identify discontinuities in the borehole walls and analyze the orientations of structural features;
- Full waveform acoustic logs to interpret compressional (P) and shear (S) wave velocities in the rock along the borehole walls, and;
- Fluid logs (temperature, conductivity, flow) to identify depths of fractures transmitting fluid within the wells.

Results of these downhole surveys are being integrated into various aspects of the project. Logs were interpreted in the field to guide the selection of screened intervals in the base of the wells. Fluid logs, rock properties, and fracture frequency information are providing knowledge and data for the development of the conceptual and numerical groundwater flow models. Gamma and resistivity logs support lithological interpretation along the boreholes. Sonic velocities and density logs relate variations in the geomechanical properties between shallow and deeper lithologies of the uppermost bedrock unit – the Paskapoo Formation.

This report summarizes the downhole geophysical data acquisition and analyses. The suite of geophysical logs from each borehole are found in Appendix A with digital datasets provided in Appendix B.

Geological and Hydrogeological Context

The study area is within a 700 km² watershed located near the town of Fox Creek in west-central Alberta, approximately 260 km northeast of Edmonton (Figure 1). The regional aquifer in this area is the Paskapoo Formation, an extensive stratigraphic unit of Middle to Late Paleocene age, composed of mudstone and sandstone in the Western Canada Sedimentary Basin. This formation, underlying much of southwestern Alberta (>65,000 km²), is the primary groundwater supply in the province and the most important aquifer system in the Canadian Prairies. Due to its heterogeneity, the Paskapoo Formation does not have a regional-scale flow system, but is dominated by local-scale recharge processes (Grasby et al., 2008).

The Fox Creek area is located near the northern limit of the Paskapoo Formation, where bedrock lithologies are comprised primarily of mudstone, siltstone and sandstone (Smerdon et al., 2016). All wells need to be cased and screened due to the soft and friable nature of the Paskapoo Formation. Existing downhole geophysical data in the area show that P-wave velocities in the shallow rock (up to 150 m depth) are low (approx. 1700 – 2500 m/s) with densities in the 2.2 – 2.4 g/cm³ range (Smerdon

et al, 2016). Hydraulic conductivities of this heterogenous formation extend over a very wide range ($10^8 - 10^{-3}$ m/s), the higher values corresponding to pumping test results, while the lower values correspond to laboratory results from core plugs containing more fine-grained sediments (Guarin-Martinez, 2022). In the study area, values inferred from specific capacity (i.e. the pumping rate divided by the maximum drawdown) using data from the provincial databases provide hydraulic conductivities ranging between 3.4×10^{-7} and 3.4×10^{-3} m/s, but most values lie between 9.2×10^{-6} and 2.4×10^{-5} m/s (Guarin-Martinez, 2022). In this industrial area, all the water wells belong to oil and gas operators. Their median depth is 60 m, and their median static water level is 24 m below the ground surface (Guarin-Martinez, 2022). Surficial sediments are typically thin (< 10 m), but can locally reach 30 to 40 m.

Borehole Drilling Program

As part of this project, nine vertical boreholes were drilled at eight drill sites ranging in depth from 35 m to 90 m (Table 1, Figure 1). Air rotary drilling was carried out by Canadian Geo & Full Metal Drilling using a 152.4 mm (6”) diameter bit. Metal surface casings were installed through the unconsolidated sediments before continuing into rock. Bags and isojars were used to collect samples of the cuttings to describe lithological characteristics of the rock and allow for the testing of targeted compounds. Upon completion of the drilling, municipal water from a tank on surface was flushed through the boreholes. The geophysical logs were then collected in the open bedrock portion of the wells, followed by the installation of PVC casing and screen inside the boring to prevent well collapse. In the first borehole, MW-6-D, 102 mm (4”) PVC casing was inserted but did not leave enough annular space to measure the depth of the sand pack around the screen. The PVC was removed and the hole was reamed with a larger bit to accommodate the 4” PVC. For subsequent boreholes, 76 mm (3”) PVC was used to provide enough annular space for the well completions. Screens (7.6 m long, the maximum length allowed in Alberta) were installed in the lower depths of the wells after a preliminary review of the geophysical logs and cuttings descriptions. Unlike typical water wells, these monitoring wells were screened in shaley intervals because more geochemically evolved groundwater was the target for this project.

Table 1 – Borehole details. bgl: below ground level, N/A: confidential location.

Well	Date Geophysically Logged	Lat (WGS 84)	Long (WGS 84)	Approx. Elevation (m asl)	Depth drilled (m bgl)	Water level during logging (m bgl)
MW-1-C	Sept 24-25, 2020	54.3675474	-117.3811861	955	51.1	38.0
MW-3-B	Sept 26-27, 2020	54.3782800	-117.1179050	869	51	6.7
MW-3-C	Sept 28-29, 2020	54.3768344	-117.0794847	852	51.4	40.7 (start) - 24.85 (end)
MW-3-D	Sept 30 - Oct 1, 2020	54.3320481	-117.0827082	883	90	20.5
MW-6-C	not logged	54.3402160	-117.1484651	858	35	-
MW-6-D	Sept 14-15, 2020	54.3402123	-117.1484852	858	51	17.0 – 18.0
MW-8-C	Sept 18-20, 2020	54.3004500	-117.2356600	935	52	17.2 - 19.7
MW-9-A	Sept 21-22, 2020	54.2855981	-117.2592642	1049	52	27.4 - 28.0
MW-10-A	Oct 4-5, 2020	N/A	N/A	838	56	4.7

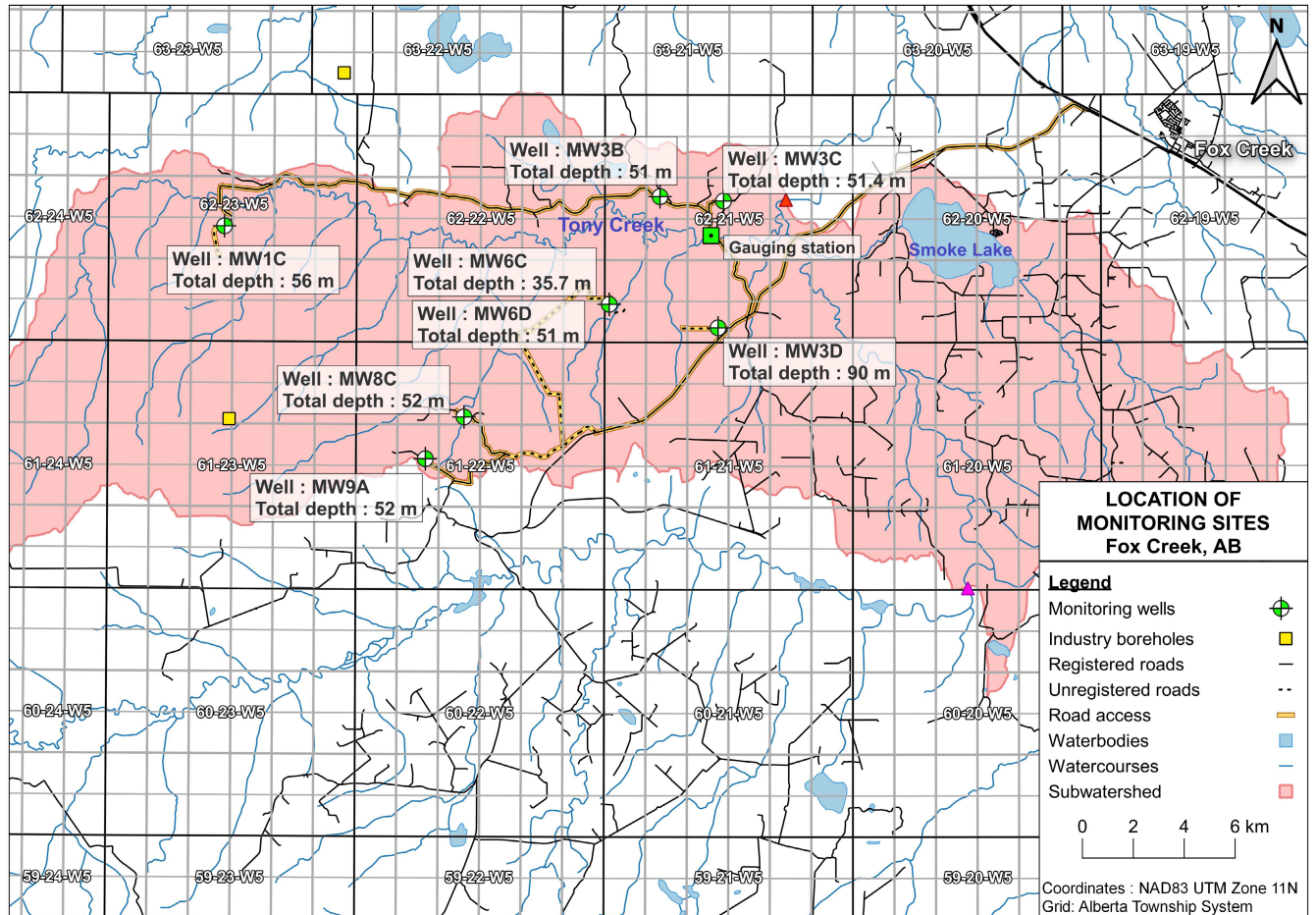


Figure 1 – Map of borehole locations logged in the Fox Creek area. The location of well MW-10-A is confidential.

Data Acquisition - Geophysical Logging

Geophysical logging was carried out by Wireline Services Group (WSG) between September 15th and October 4th, 2020. Covid restrictions prevented the GSC from travelling to site. Risk of borehole collapse or obstruction increased the longer the wells remained open. Therefore, logging began right after the drilling ended and was often completed before water levels or fluid temperatures were able to stabilize in many of the boreholes.

The tool suite consisted of eight instruments including natural gamma, gamma-gamma density, video camera, acoustic televiewer (ATV), full waveform sonic (FWS), normal resistivity, fluid temperature/conductivity, and heat pulse flow meter for boreholes with vertical flows less than 4 L/min (Table 2). An impeller flow meter was also deployed in three boreholes with higher flows, but was found to be too noisy during post-processing to be reliable, and results are not reported further. Due to the potential instability of the boreholes, a dummy probe was the first tool deployed to ensure an open hole, followed by the fluid temperature/conductivity tool. As the wells contained at least some municipal water introduced during the drilling and flushing, at three of the wells another fluid log was collected during the next shift (2.5 hrs to 19 hours later, with other tools run between fluid logs). This allowed for a comparison of the logs to identify depths where fluid conditions were changing as the fluid in the hole stabilized. The camera log was then used to examine the condition of the walls for stability,

fluid clarity, and signs of fluid movement (e.g. depths of water in-flow, or direction of particle movement in water). The FWS, natural gamma, and resistivity were generally run in any order (as shift time permitted), followed by the gamma-gamma density once borehole stability was confirmed. The flow meter was run last, as this test was most time consuming and required a review of all the data to optimize the selection of stationary test depths. During the logging, the GSC provided remote support to WSG in choosing flow meter test depths. As a last step, after review of the preliminary geophysical data, and in consultation with the team on site, the GSC selected the depth interval for the PVC screens.

Camera inspections revealed a range of bedrock wall conditions from smooth to rough to highly fractured and/or collapsed. As some of the wells were not stable enough for logging with all of the tools, Table 3 outlines the logs collected in each open well. Additionally, some electrical interference with the heat pulse flow meter was experienced in wells MW-6-D and MW-8-C, and corrected when a different winch was brought to site.

Table 2 – Borehole instruments used for the Fox Creek surveys.

Tool	Instrument
Borehole Video Camera	R-CAM 1000 Video Inspection System
Full Waveform Sonic	Electromind FWS60
Acoustic Televiwer	Electromind BHTV42G
Gamma-gamma Density	Century 9238 Compensated Density (Cs ¹³⁷ , 168 milliCuries)
Fluid temperature/Conductivity	Mount Sopris QL40-FTC
Natural Gamma	Mount Sopris QL40-GR (polyprobe with FTC)
Resistivity	Mount Sopris Q40RES-1000
Flow Meter – Heat Pulse	Mount Sopris HFP-2293

Table 3 – Summary of log types collected in each well. Due to rough/fractured walls, the density tool was not run in wells MW-6-D and 9-A, and sonic was not run in 9-A.

Well	Camera	Gamma	ATV	Density	Sonic	Resist.	Fluid logs	
							Temp/Cond	Heat Pulse Flow Meter
MW-1-C	✓	✓	✓	✓	✓		✓	✓
MW-3-B	✓	✓	✓	✓	✓	✓	✓	✓
MW-3-C	✓	✓	✓	✓	✓	✓	✓	✓
MW-3-D	✓	✓	✓	✓	✓	✓	✓	✓
MW-6-D	✓	✓	✓		✓	✓	✓	
MW-8-C	✓	✓	✓	✓	✓	✓	✓	✓
MW-9-A	✓	✓	✓			✓	✓	
MW-10-A	✓	✓	✓	✓	✓	✓	✓	✓

Data Processing and Analyses

Calibration

Post-survey tool calibrations of the dual sensor density and fluid temperature/conductivity tools were carried out by WSG at the GSC's Borehole Calibration Facility in Ottawa, ON, on October 10, 2020. Other tools (FWS, ATV, resistivity, flow meter, natural gamma) were factory calibrated and found to be operating within specifications at the WSG workshop.

Three repeat density runs in the GSC's calibration bedrock borehole (BC81-2) were compared to core calibration datasets provided by the GSC (Crow et al., 2021) over a range of rock types and densities spanning 2.44 to 3.05 g/cm³. Density tool calibration constants were adjusted for the long and short-spaced sensors, achieving an ultimate R² value of 0.96 when comparing core and corrected probe densities (WSG, 2020). These calibration constants were retroactively applied by WSG to the density data collected in Fox Creek.

The fluid temperature/conductivity tool responses were also compared to GSC calibrated handheld sensors (Thermaprobe TL1-R, Oakton CON6+ fluid conductivity meter) in ice water and warm water baths provided by the GSC at the Ottawa calibration facility. The results indicated close agreement of the temperatures in the ice bath (1.27°C downhole probe versus 1.76°C calibration) and warm water bath (17.78°C downhole probe versus 17.93°C calibration). The conductivities, compensated to a common reference temperature of 25°C, indicated a low point of (133 µS/cm downhole probe versus 160 µS/cm calibration) and a higher point of (498 µS/cm downhole probe versus 467 µS/cm calibration). The tool was found to be operating within specifications for both temperature and conductivity, and these results were found to be acceptably accurate for the surveys.

Log data (natural gamma, resistivity, ATV amplitude image, corrected density, 1-arm caliper, and fluid temperature/conductivity) were assembled into composite WellCAD log suites with well metadata by WSG for delivery to the GSC. Data were checked by WSG for depth consistency amongst logs and were reported to need little to no adjustment.

Processing

The GSC conducted analyses on the ATV, FWS, and heat pulse flow meter logs. ATV data were provided to the GSC oriented to magnetic north as exported from LIM processing software (developed for Electromind logging tools). Similarly, FWS logs were exported from LIM software as three separate .sg2 files – one for each receiver. Heat pulse flow meter data were provided as raw log files. GSC processing was carried out using WellCAD software (v5.5). Final processed data were assembled into log suites by the GSC, provided in Appendix A.







Acoustic Televiewer and 360° caliper

ATV images were imported into the WellCAD image processing module as amplitude and traveltimes logs. The 3D borehole diameter was computed from the traveltimes log prior to interpreting structural orientations from the amplitude image. As the transmitted acoustic signal could be attenuated or scattered in broken zones, traveltimes less than 2200 µs in the rock (equivalent to the traveltimes inside the casing) were interpreted as an early mispick of signal arrival from the tool's acoustic window and removed. Additionally, tool tilting in some extremely broken intervals caused bands of uneven (too high and too low) traveltimes which couldn't be corrected with centralization routines and were therefore removed from the caliper calculation. Borehole diameter was calculated using a borehole fluid

velocity of 1450m/s (producing the best match with the known metal casing diameter of 165 mm in the overburden), and displayed as minimum, maximum, average caliper logs. Having the three borehole diameters enhances the interpretation of structural features, as a continuously open fracture will increase in diameter in the minimum log as well as the maximum.

An empty structure log was created in the software, linked to the average caliper log, and laid over the amplitude image. The unwrapped images of the borehole wall cause planar features to appear sinusoidal. Sinusoids were fit to these features in the structural log and classified according to Table 4. Dip angles of the structures were then corrected for minor borehole tilt from vertical as measured by the ATV’s tilt meter. “Open” features could be further classified as features with data supporting water movement, based on the observation of a deviation in the fluid temperature/conductivity logs and/or changes in flow meter rates above/below the feature. It should be noted that fluid can move through a fracture and not cause a significant temperature, conductivity, or flow anomaly, so these interpretations may not capture all transmissive features intersected by the borehole. Additionally, wall roughness caused by the rotary drilling causes feature classification to be more interpretive than in sooth-walled cored holes.

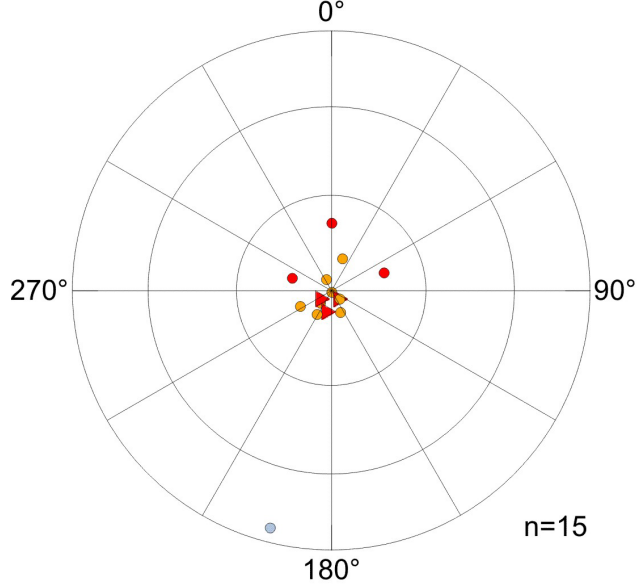
Table 4 – Structural classifications

Structure Type	Structure Sub-type	Structure Code*	Tadpoles (no indication of flow)	Tadpoles (log data support water movement)
Open Features	Open bedding planes	OB		
	Open joints	OJ		
Closed Features	Closed bedding planes	CB		—
	Closed joints	CJ		—

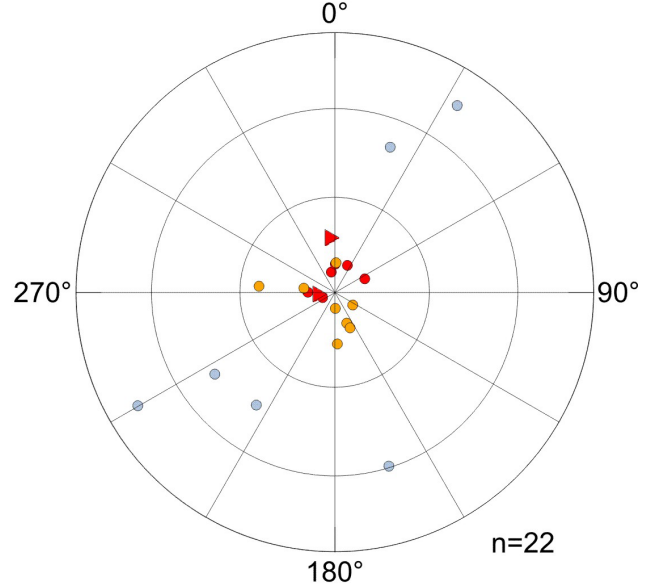
* Codes for structures which are interpreted as transmitting fluid are followed by a “-F”.

Data were subsequently corrected for declination (15.86°E in Sept 2020; <https://www.ngdc.noaa.gov/geomag/calculators/magcalc.shtml>) for stereogram presentation in WellCAD. Planar structural features were plotted as points on stereograms, representing poles after plane projection on the lower hemisphere of an equal-area Schmidt diagram (Figure 2). Structures are provided in tables relative to magnetic north and true north in Appendix B.

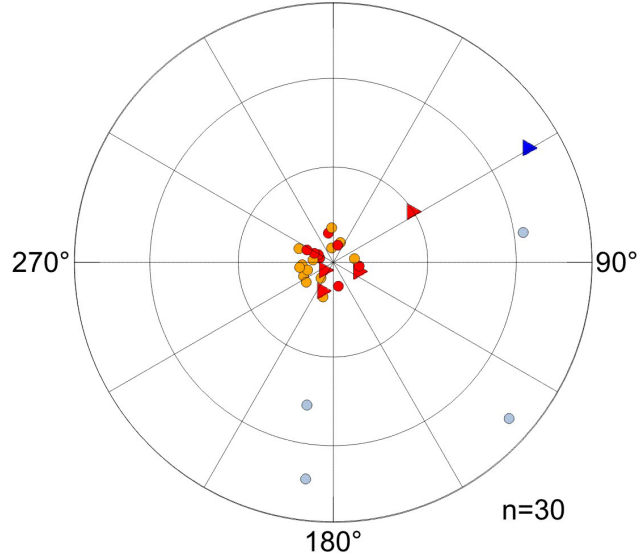
Schmidt Plot - MW-1-C



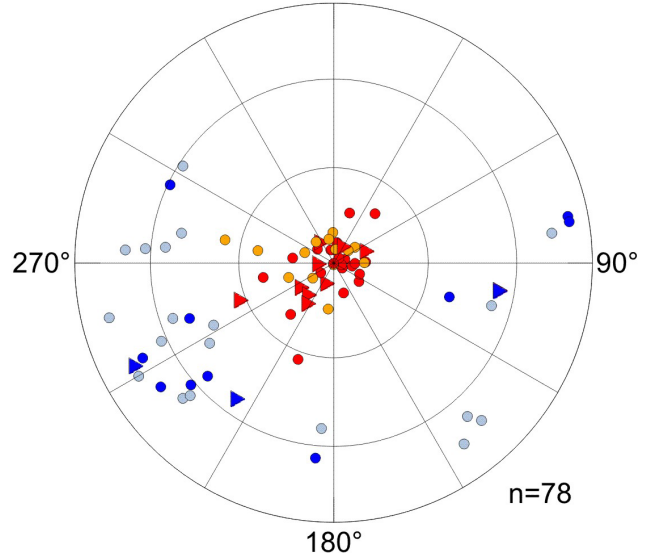
Schmidt Plot - MW-3-B



Schmidt Plot - MW-3-C



Schmidt Plot - MW-3-D



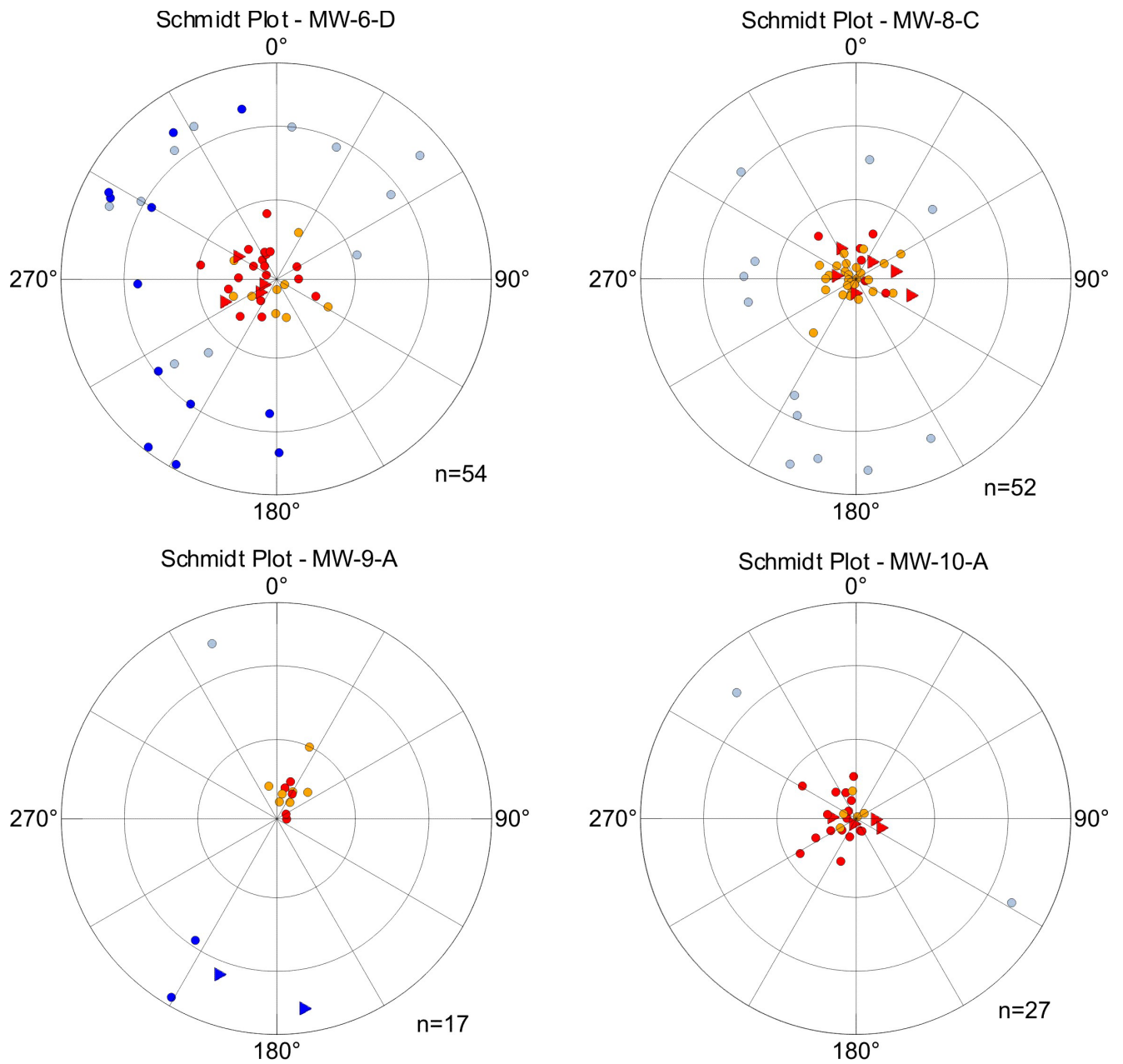


Figure 2 – Stereonets (equal area Schmidt plots, lower hemisphere projection, corrected to true north) based on structures interpreted from acoustic televiewer logs. Poles are colour-coded based on Table 4.

Full waveform sonic logs (P- and S-wave velocities)

FWS logs were shifted to their original depth relative to the transmitter prior to velocity analyses in the WellCAD FWS processing module.

P-wave velocities were computed in two ways:

- 1- from transit times using a first arrival picking algorithm on receivers 1 and 2 with manual corrections as required, and
- 2- using a velocity analysis technique called semblance processing, which looks for similarities in waveforms across all three receivers.

A picking algorithm was optimized for this dataset, creating a well log containing the first arrival intercept times of receivers 1 and 2 (Figure 3). Manual intervention was required in few instances to correct algorithm mispicks. The arrivals were clear and the waveforms were not filtered prior to picking. The transit time between the two receivers was divided by the distance between them (0.30 m) to give the P-wave slowness (DTP, $\mu\text{s}/\text{m}$). P-wave velocity (m/s) was computed by taking the inverse of the slowness ($V_p=10^6/\text{DTP}$).

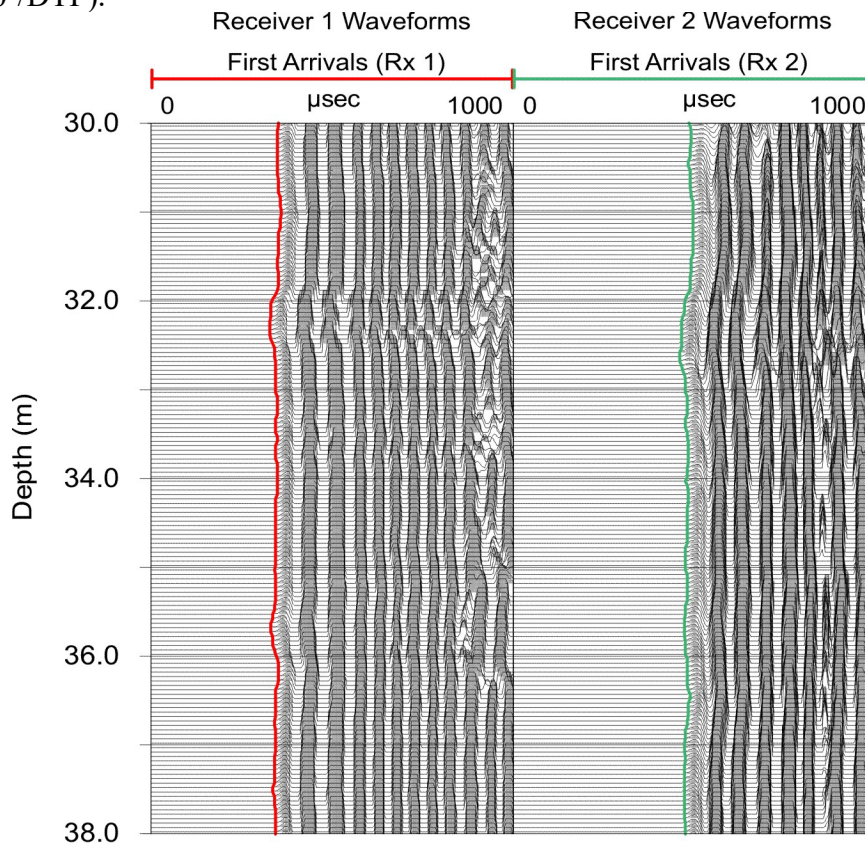


Figure 3 – Waveform data from well MW-3-C showing first arrival picks (red and green traces) on waveforms from Receivers 1 and 2.

A second technique called semblance processing was used to determine the slowness of P- and S-waves across all three receivers. Paillet and Cheng (1991) provide a description of the semblance cross-correlation technique developed for sonic data in an open borehole. The semblance algorithm starts with an assumed slowness and computes a coherence value for the waveform across the three receivers, then moves on to the next record (Figure 4A). A velocity analysis plot (coherence maxima versus record depth) was generated and used to analyse the slowness of the refracted P- and S-wave head wave slownesses (Figure 4B). A bandpass filter of 5-10-35-40 kHz around the tool's frequency of 12 - 15 kHz was found to remove low frequency noise and sharpen the P- and S-wave coherence. P-wave slowness from both approaches are shown superimposed in Figure 4. Although the semblance approach smooths out the peaks and troughs present in the first arrival picking approach, the two approaches were in close agreement.

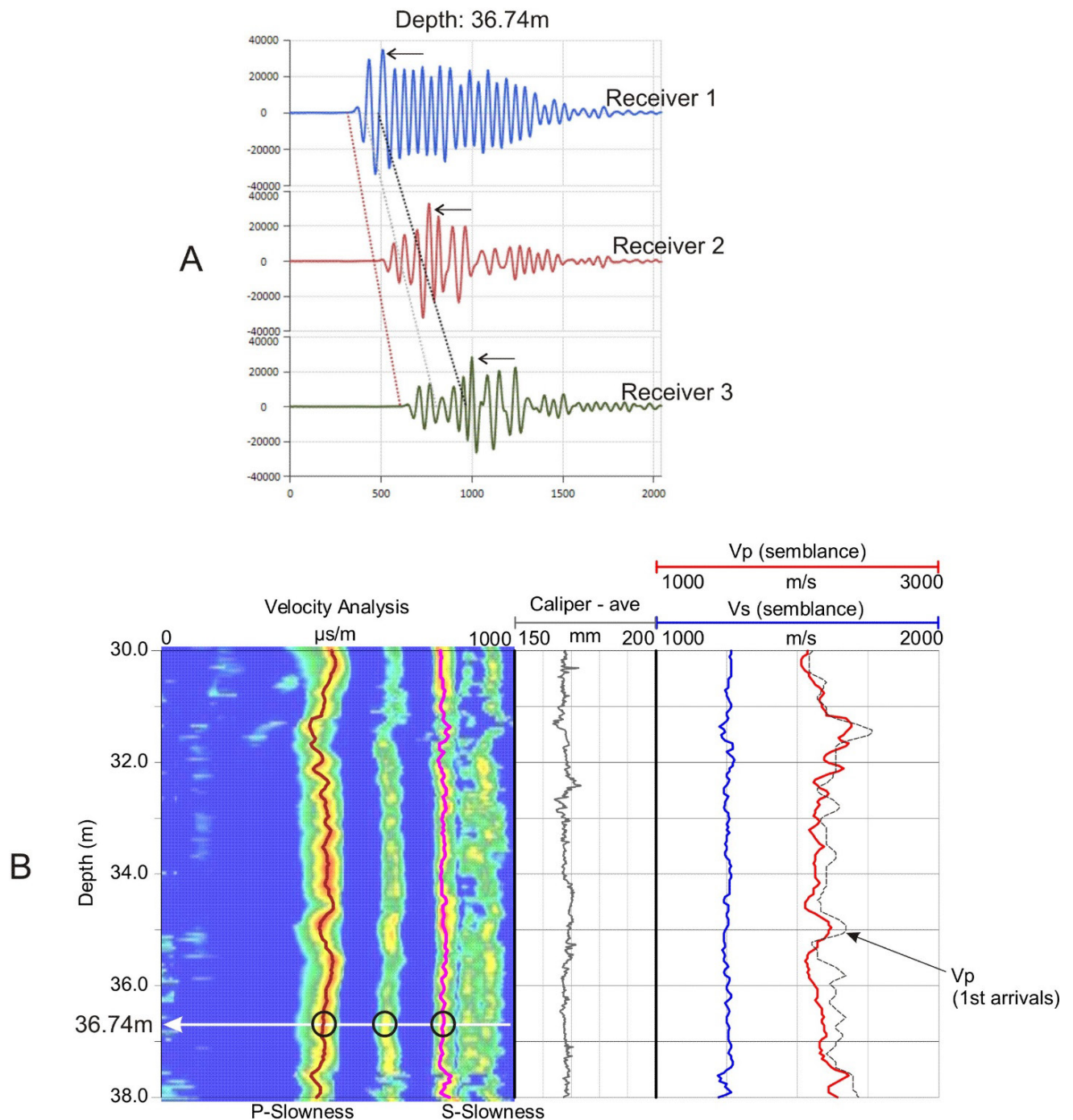


Figure 4 – Waveforms and semblance velocity analyses in well MW-3-C. (A) Traces recorded by the three receivers simultaneously at 36.74 m. Dotted lines represent the slowness of similar waveforms expressed as the ratio of time and distance (given in $\mu\text{s}/\text{m}$). (B) Semblance velocity analysis combining all the traces collected along the borehole wall (left panel). Circles along the arrow at 36.74 m show how the three dotted lines in (A) are represented in the velocity analysis plot. The caliper log (center panel) supports the interpretation by identifying fractures or intervals of rough walls. P and S wave slowness are used for velocity log calculations (right panel). Vp logs from first arrival and semblance analyses are overlaid for comparison.

The interpretation of S-wave slowness (DTS) can be challenging in conditions where rough walls (here produced by the rotary drilling techniques) can negatively interfere with the propagation of waveforms along the borehole wall (Crow et al., 2017). In this dataset, a second maxima (generally associated with S-wave slowness) is too early in time to produce a Poisson's ratio in the usual range for sandstones. Poisson's ratio (ν) is a dimensionless elastic modulus computed from DTS and DTP that predicts how a rock will expand in a direction perpendicular to an applied stress, ranging between 0.0 and 0.5 for most materials. Although literature provides a wide range of ν values in sandstones, it is rarely reported below 0.1 (typically ranges between 0.2 and 0.35 in sandstones, e.g. Gercek, 2006). Picking the second maxima (see Figure 4B) produces a ν around 0 (± 0.1). The third maxima is associated with a later arriving and higher amplitude waveform (shown by black arrows in Figure 4A) and provides a more reasonable DTS, producing a ν dataset that ranges from 0.10 to 0.45 (when fractured intervals are removed) with a mean of 0.27 (Figure 5). It should be noted this is a non-standard interpretation of DTS (or Vs) from semblance processing, and may be indicative of DTS times merging with tube waves travelling along the borehole walls, and therefore should be used with caution.

In 2022, the GSC drilled three new cored holes, two of which are adjacent to boreholes with FWS and density logs (MW-3C and MW-8C). The new cored holes were labeled MW-3E (15 m from MW-3C) and MW-8D (6 m from MW-8C). Eight core samples of various material types were selected to support calibration of the geophysical logs and sent to Core Laboratories in Calgary, Alberta for routine core analyses (ambient porosity, ambient air permeability, grain density, and bulk density) and dynamic ultrasonic tests (unconfined P and S wave velocity, Bulk/Young's/Shear moduli, and Poisson's ratio). The results of the unconfined ultrasonic testing for the S-wave arrivals were inconclusive (unclear first arrivals), so the tests were rerun on new sample plugs under increasingly greater levels of confinement until an S-wave arrival could be interpreted. Results of the relevant core tests are presented in Table 5, and displayed alongside the velocity and density logs from MW-3C and MW-8C in Appendix A.

The core densities are in close agreement with the downhole logs ($R^2=0.99$, core density = $0.96 \times \log$ density) for all material types. The core velocities are both higher and lower than those interpreted from the downhole logs and appear to be influenced by material type. In the finer-grained intervals of borehole MW-3E (mudstone-siltstone), the core Vp and Vs are both higher than those measured downhole (approximately 10 – 20% for the unconfined samples) – a result anticipated in rough borehole wall conditions. A sandstone plug in MW-3E was taken from a cemented bed and had a higher Vs than the downhole log (20%), but a much lower Vp (approximately 50% lower) than the downhole log. This may be indicative of chemical changes occurring in the cements when core is removed from saturated conditions in situ; cements are discussed in more detail in Lavoie et al., 2023. A second plug in friable sandstone failed during analyses. The core plugs taken from MW-8D indicate a range of responses in the sandstones that are both higher and lower than the downhole logs (Vp, -65% to +5%; Vs, -40% to 20% for the unconfined samples, improving with modest confinement, Vp, -15% to 15%; Vs, -40% to 5%). The variation between core and logs could be due to factors including rough borehole walls, scale of test methods (sub-m vs. sub-cm), and alteration effects in core plugs of different material type, compaction and cementation.

Despite this velocity variability, the Poisson's ratios from the core tests are within the range of values interpreted from the downhole logs (Figure 5), providing some support for the log interpretation methodology discussed above. The effect of confinement on the samples tends toward a slight increase in PR. Difficulties encountered in both downhole and core testing methods due to the soft and friable nature of the Paskapoo Fm indicate that shear displacement in these shallow sandstones can be difficult

to measure, and mechanical properties relying on Vs (shear and Young’s modulus) should be interpreted with caution; multiple test methods are recommended as a means of comparison.

Table 5. Results from Core Laboratories testing in 2023; material descriptions from Lavoie et al., 2023. Bulk density measured as received.

Sample Number	Material type	Mid-sample depth (m)	Bulk den. (g/cm ³)	Vp (m/s) 0 MPa Conf. Pres.	Vs (m/s) Conf. Pres.	Conf. Pres. (MPa)	Vp (m/s)	Vs (m/s)	PR Unconfined/ Confined
MW-3E-3	Shale-mudstone-siltstone	31.21	2.32	2690	1490	13.79	3149	1746	0.28 / 0.28
MW-3E-4		34.15	2.40	2507	1543	1.38	2632	1548	0.20 / 0.24
MW-3E-6		36.12	2.42	2660	1518	0.69	2732	1528	0.26 / 0.27
MW-3E-9	Cemented sst	44.13	2.60	2829	1894	2.76	3324	2103	0.09 / 0.17
MW-3E-10	Friable sst	48.10	2.16	Failed during analysis					
MW-8D-4	Sandstone – shaly, conglomerate	22.45	2.16	1277	855	5.52	1808	1194	0.09 / 0.11
MW-8D-5		24.03	2.24	1693	1119	11.03	2274	1490	0.11 / 0.12
MW-8D-6	Shale-mudstone-siltstone	29.5	2.44	2424	1557	5.52	2591	1726	0.15 / 0.10

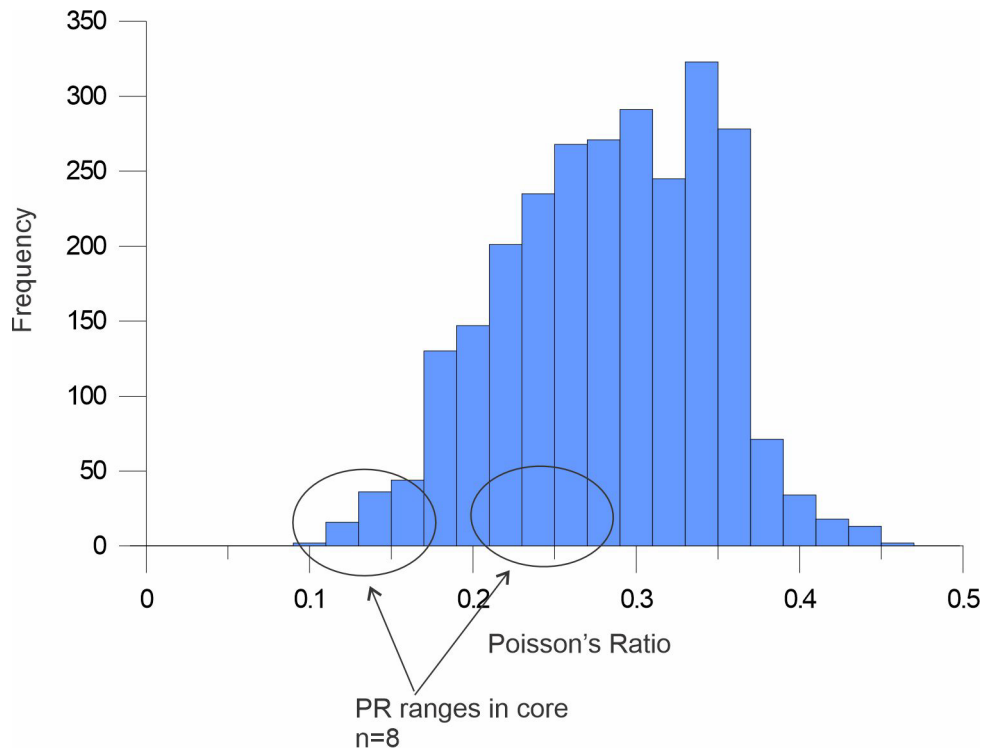


Figure 5 – Poisson’s ratio distribution.

Calculated Mechanical Properties

Common mechanical parameters of rock such as dynamic Poisson's ratio (ν) and dynamic Young's modulus (E) can be calculated from sonic log measurements (V_p , V_s , km/s) and density logs (ρ , g/cm³). As mentioned above, ν is a dimensionless elastic modulus computed using V_p and V_s . In general, the relationship between V_p and V_s depends on several factors, including matrix material, degrees of saturation and consolidation, differential pressure (confining pressure minus pore pressure), porosity, and other factors such as geometry (Lee, 2003). Poisson's ratio can be calculated using the formula (Saxena, Krief, and Adam, 2018):

$$\nu = \frac{V_p^2 - 2V_s^2}{2V_p^2 - 2V_s^2} \quad [1]$$

E is a measure of the stiffness of a material and can be computed when both sonic logs and density logs are available. E is typically expressed in units of GigaPascals (GPa) as (Saxena, Krief, and Adam, 2018):

$$E = \rho V_s^2 \frac{3V_p^2 - 4V_s^2}{V_p^2 - V_s^2} \quad [2]$$

Cross plots of E versus ν are commonly used in geomechanical assessments of rock units. High ν and low E correspond to more ductile rock, while low ν and high E are more characteristic of brittle rock. Cross plots of the moduli are presented in the coming section.

Flow meter data

The heat pulse flowmeter (HPFM) is designed to measure vertical borehole flows between 0.1 – 4 L/min. The tool contains a heating grid with equidistant temperature sensors positioned a few centimetres above and below the grid. Rubber diverter petals centralize and seal the probe in the borehole, forcing the fluid to pass through a wire mesh over the heating grid and the sensors. When the tool is in position for a series of stationary readings, a heat pulse is triggered by the operator. The grid heats a lens of water that moves up or down with the flow of the borehole fluid past the thermistors. An amplifier detects the difference in temperature between the sensors, and converts the output to a frequency which is sent up the cable and recorded by the logging software. The software records the time elapsed between the heat pulse trigger and the measured peak temperature change, which is converted to flow from manufacturer calibration values.

Data were processed using the MatrixHeat software (v3.2). Heat pulse waveforms were analysed for similarity across a minimum of three subsequent pulses over a period of (at least) 10-15 minutes to allow the fluid to settle between instrument moves. These averaged flow values are represented by a black dot in the log suites in Appendix A and provided in spreadsheets in Appendix B. In some intervals, flow values were inconclusive. This could be caused by a poor diverter petal seal in the borehole, or flows above/below the flow meter's threshold, making a waveform pick unclear. In these cases, other log data were used to assist in the interpretation of flow (video logs capturing particle movement, fluid temperature/conductivity logs). Unclear or low confidence flow responses are represented by a grey dot in the log suites.

Interpretation

Lithological Observations

Stratigraphic descriptions developed from examination of the cuttings during the drilling (Figure 6) are plotted alongside the geophysical logs in the log suites (Appendix A). The geophysical logs indicate that physical properties varied in each borehole and, as might be expected in a fluvial sandstone and mudstone complex, marker horizons could not be traced from well to well.

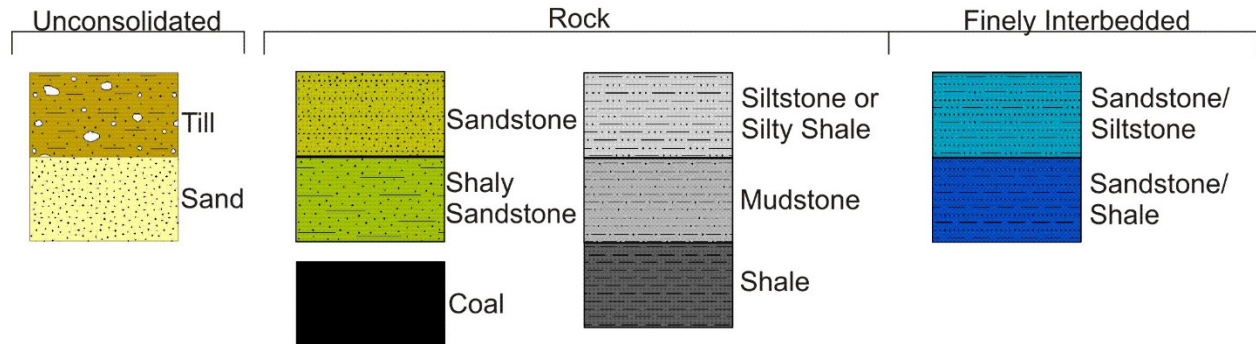


Figure 6 – Material classifications plotted alongside geophysical logs.

Generally, the rock described as more shale-rich produced relatively higher gamma counts and lower resistivities than the other shale-poor rock types. Gamma count variation along the boreholes tended to be gradational rather than abrupt at bed boundaries.

In the seven boreholes where FWS and ATV logs were collected, the geophysical logs identify 25 beds of relatively elevated velocity and acoustic reflectance (along with elevated density and resistivity, where available), interpreted to be cemented (Figure 7, Table 6). These beds have an average thickness of $0.50 \text{ m} \pm 0.25 \text{ m}$. More cemented beds likely exist, but were undetected if located above the water level in the boreholes, or if their bed thickness was less than approximately 0.25 m. The majority (20) of these responses were in intervals described as sandstone and two were in siltstone. The remaining three were in shale (MW-3-D) but based on the low gamma responses in these intervals, were likely cemented sand or siltstone beds that weren't differentiated during the describing of cuttings (Figure 7, red arrows).

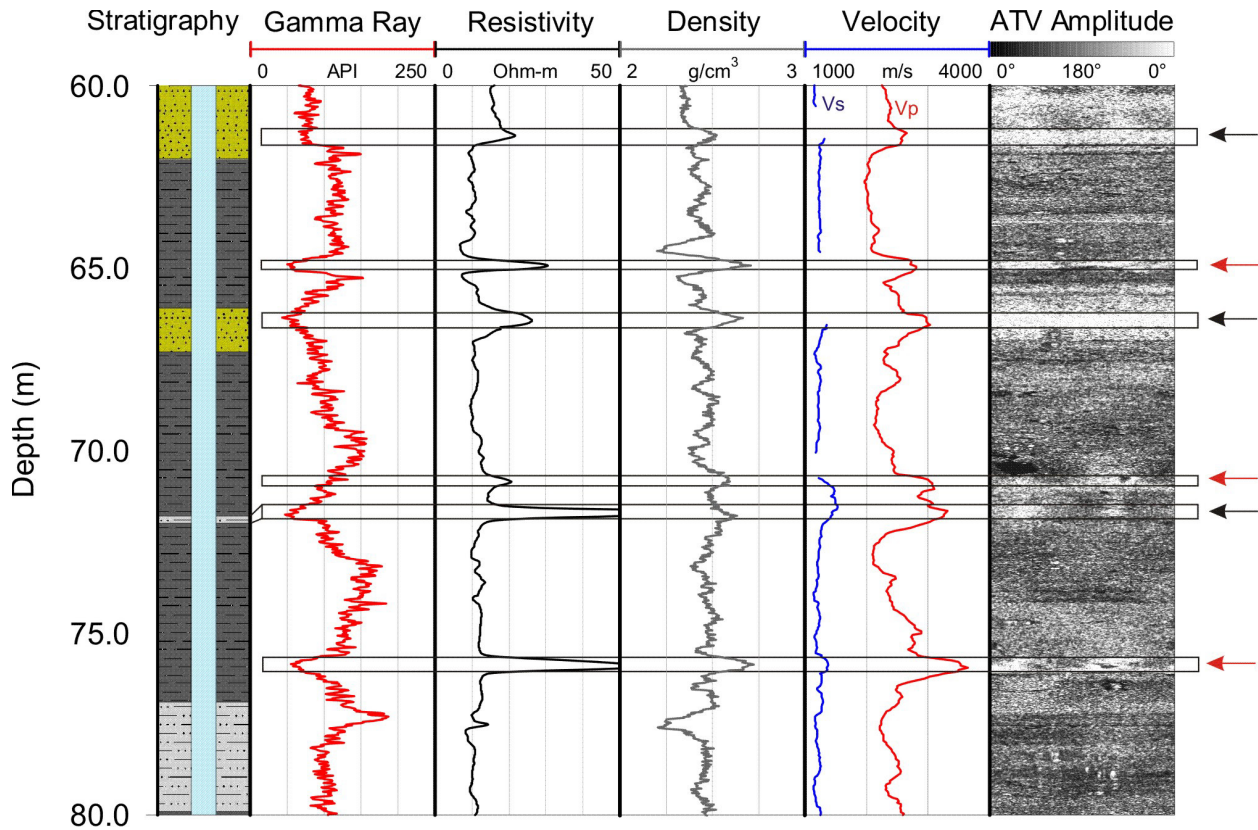


Figure 7 – Boxes identify intervals with reduced gamma counts and elevated resistivity, density, and velocity values. The televiwer image indicates these intervals have an increase in acoustic reflectance. These intervals are interpreted as more cemented than the surrounding beds, and may have implications for localized groundwater flow. Red arrows indicate interpreted beds of silt or sandstone within the thicker shale interval.

Various rock textures within the main rock types can be observed along the borehole walls. They range from massive and smooth in appearance (Figure 8A), to finely bedded and rough (Figure 8B). The interaction of the drill bit with the rock and weaknesses/fracture planes within lead to a range of wall conditions from open bedding planes, to complete collapse of the borehole wall (Figure 8C). These more fractured intervals can influence the geophysical log data, as many of the tools have sensors that need to come in contact with the borehole wall (density, resistivity), transmit acoustic signals along the wall (FWS), or reflect signal off the wall (acoustic televiwer). In intervals where caliper logs indicate significant fractures caused decreases in density or velocity, these intervals were removed from the dataset for calculation of physical and geomechanical properties. This amounted to a removal of 13 - 14% of the dataset for Vp (25.1 m from 185.6 m) and density (21.7 m from 154.1 m), and 29% of the dataset for Vs (54.0 m from 185.6 m), where the interpretation of Vs was particularly sensitive to rough-walled intervals.

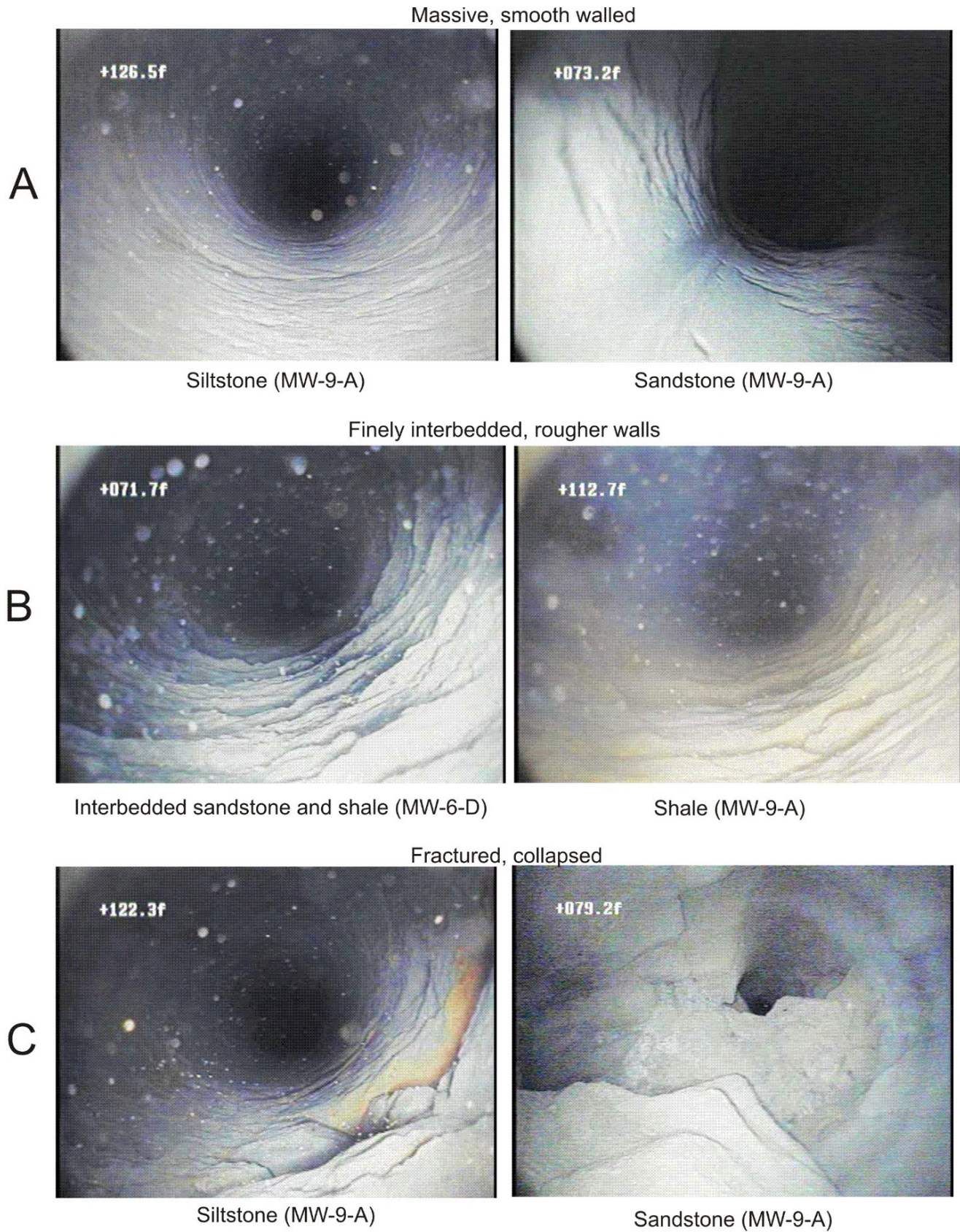


Figure 8 – Textures and conditions observed in the borehole walls. Note appearance of iron staining on fracture plane in lower left image (MW-9-A, 122.3 ft (37.3 m)).

Preliminary Structural Observations

ATV logs recorded 227.4 m of the 315.0 m of rock drilled (72%). Since the ATV can only record data in fluid, the missing 87.6 meters (28%) are primarily above the water level, or, obscured by metal casing drilled into the top of rock. A compilation of structural features identified below the water level in all eight boreholes indicates relatively flat-lying bedding (n=208) with maximum dip angles reaching 35°, but most bedding planes (80%) are dipping 15° or less. The average dip of all the bedding features selected is 2.3° with an average azimuth of 113° (Figure 9). Of all bedding planes, 87 (42%) are interpreted to be open, and of these, 25 (12%) have data supporting evidence of water movement. In rough borehole walls, fractures cannot always be clearly observed, and the assessment of flowing fractures can be more difficult than in smooth-walled boreholes (i.e. diamond drilled in more consolidated rock). All open fractures represent secondary permeability features that may act as preferential flow paths, even if they are not designated as “flowing”.

Joints (n=87) had dip angles ranging from 32° to 90°. Of the 30 features (34%) interpreted to be open, only six joints were interpreted to have vertical flow (in wells MW-3-D and -9-A), suggesting that the majority of the fluid transmitted into/out of the wells along discontinuities was through open bedding planes. Dip directions of the joints were random, with a mean dip of 65.

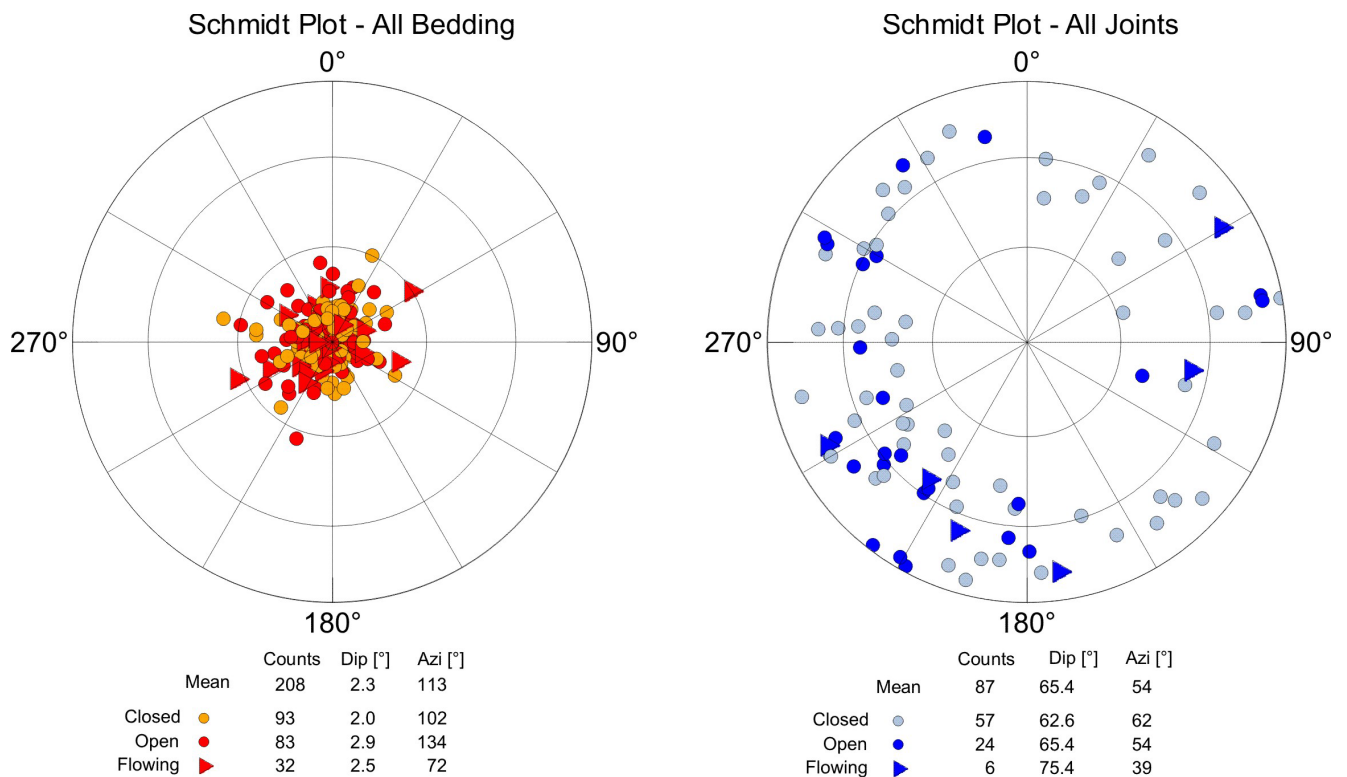


Figure 9 – Stereonets compiling bedding and joints from all eight boreholes.

Geomechanical Properties

Physical properties and elastic moduli of the near surface bedrock are summarized in Tables 6 and 7. Values were calculated using the sonic velocities and density logs after intervals affected by significant fractures in the borehole walls were removed, as assessed by the caliper and ATV amplitude logs. Stratigraphic boundaries are based on cuttings descriptions and are therefore subject to some errors in contact depths and thin bed resolution.

Velocity and Density ranges by rock type

The mean density among all rock types, as measured by the long-spaced detector (in borehole fluid), was $2.39 \pm 0.10 \text{ g/cm}^3$. The lowest densities, on average, were measured in the sandstones ($2.35 \pm 0.08 \text{ g/cm}^3$) once the influence of the cemented beds was removed. Rock types containing shale-sized particles (shale, silty shale) had higher densities (2.42 ± 0.08 and $2.44 \pm 0.06 \text{ g/cm}^3$, respectively). These results support the interpretation that the sandstones are more porous and thus likely more permeable than the rock types containing finer grain sizes. Conversely, the mean density in the cemented beds increases to $2.53 \pm 0.06 \text{ g/cm}^3$ (reaching a maximum of 2.71 g/cm^3), suggesting a reduced porosity and permeability, an observation borne out by the core plug tests. These cemented beds may represent localized barriers to vertical flow, but the lateral extent of these beds away from the boreholes, or their degree of fracturing, is not known. Mudstones (found in MW-1-C and MW-10-A) had relatively lower densities but were found in fractured intervals and may be influenced by wall conditions. The rock types with fewer than 10 readings (finely interbedded sandstone/siltstone and coal) were not considered statistically significant. The coal beds (<10 cm) were thinner than the vertical resolution of the tools, and physical properties therefore reflect the influence of the surrounding rock types.

Velocities are fairly consistent among the rock types, and the mean V_p follows the density trends. The V_s does not always follow this trend, and likely reflect challenges in the interpretation of V_s in these borehole wall conditions.

Elastic Moduli

Summary statistics from the calculations of Poisson's ratio (ν) and Young modulus (E) are presented in Table 7 and plotted in Figure 10. The Poisson's ratio spans a wide range of values which reflects the variability of the sediments and their porosity/compaction/degree of fracturing, but which is also induced by the conditions of the borehole wall and challenges in the interpretation of V_s in these wells. A low value of V_s would result in an underestimation of in situ E, a result predicted by the core plug tests. A group of data points with higher values of E are circled on Figure 10A, representing the response within the higher velocity/density beds.

In reservoir rock mechanics, a negative correlation typically exists between ν and E, where a low ν and high E indicates a more brittle behaviour, and a high ν and low E is more indicative of ductile behaviour (e.g. Grieser and Bray, 2007). In the monitoring wells, the E- ν correlation appears to be slightly positive (Figure 10A). The majority of the data are centered around a ν of 0.27, with a tail that extends toward lower values, a results also seen in the core ultrasonic tests. The lower values of ν tend toward more broken or softer intervals (where V_p dips and V_s resolution drops), which would also have lower densities, producing a lower E. Therefore, this correlation is likely a response to various lithological factors (porosity, fractures, softer rock, shallower depths and thus lower confining pressures) and borehole wall conditions (roughness leading to complications in the interpretation of DTS).

Table 6 – Density and velocity by rock type. Dashes indicate the tool did not collect data within these rock types. ‘N_o BH’ indicates the number of boreholes where this rock type was logged with geophysical instruments. Grey text indicates too few data points for assessment.

Rock type	No. BH	Density (g/cm ³)		V _p (m/s)		V _s (m/s)	
		Mean ± 1 SD	# Pts (Interval logged)	Mean ± 1 SD	# Pts (Interval logged)	Mean ± 1 SD	# Pts (Interval logged)
All types	7	2.39 ± 0.10	2648 (132.4m)	2270 ± 335	3211 (160.6m)	1240 ± 50	2633 (132.6m)
All Sandstone	7	2.37 ± 0.10	1468 (73.4m)	2270 ± 415	1552 (77.6m)	1250 ± 60	1056 (52.8m)
- cemented beds removed		2.35 ± 0.08	1308 (65.4m)	2200 ± 325	1389 (69.5m)	1240 ± 40	976 (48.8m)
All Shale	3	2.43 ± 0.08	988 (49.4m)	2280 ± 255	988 (49.4m)	1240 ± 45	911 (45.6m)
- cemented beds removed		2.42 ± 0.08	960 (48.0m)	2255 ± 205	960 (48.0m)	1235 ± 40	886 (44.3m)
Cemented beds (SST, SLST, SH)	7	2.53 ± 0.11	196 (9.8m)	2910 ± 520	207 (10.4m)	1340 ± 125	121 (6.0m)
Siltstone/silty shale	2	2.44 ± 0.06	93 (4.6m)	2415 ± 170	93 (4.6m)	1200 ± 50	93 (4.6m)
Mudstone	2	2.36 ± 0.11	80 (4.0m)	2220 ± 200	80 (4.0m)	1255 ± 55	78 (3.9m)
Shaly Sandstone	1	-	-	2400 ± 180	180 (9.0m)	1230 ± 35	180 (9.0m)
Interbedded Sandstone/Shale	1	-	-	2150 ± 175	299 (15.0m)	1235 ± 25	299 (15.0m)
Interbedded Sandstone/Siltst.	1	2.34 ± 0.05	9 (0.4m)	2200 ± 85	9 (0.4m)	1200 ± 10	9 (0.4m)
Coal (thin beds)	2	2.33 ± 0.05	10 (0.5m)	1940 ± 65	10 (0.5m)	1225 ± 10	6 (0.3m)

Table 7 – Summary of Poisson’s ratio (ν) and Young’s modulus (E) calculations from geophysical logs.

	Poisson’s Ratio (n= 2627)	Young’s Modulus (GPa) (n= 2062)
Mean	0.27	9.50
Median	0.27	9.32
Standard deviation	0.06	12.80
Min	0.05	7.30
Max	0.45	19.20

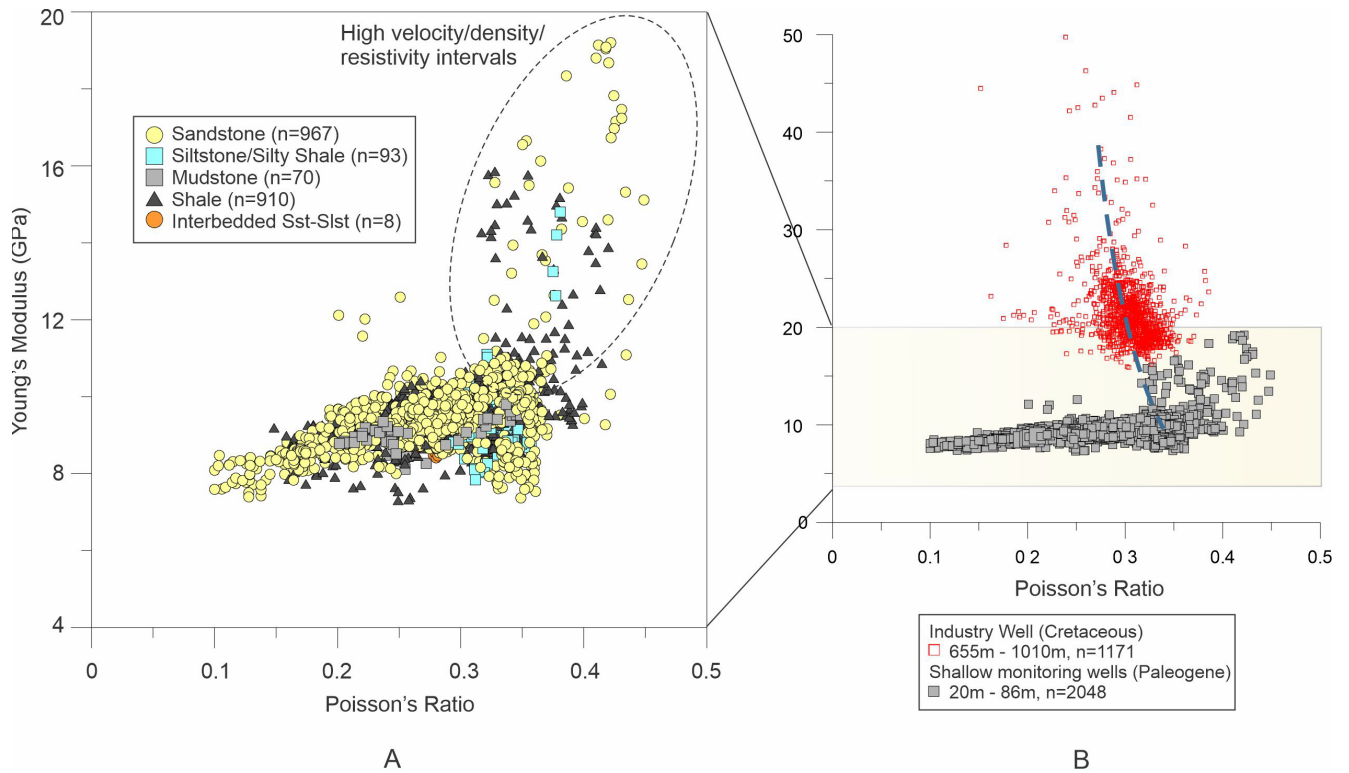


Figure 10. A) Cross plot of Young's modulus versus Poisson's ratio for shallow bedrock (20 m – 86 m deep). Circled data points with higher velocities and densities, lying outside the general trend of the dataset, are interpreted as being cemented. B) Monitoring well dataset (grey points) plotted with deeper industry well data in study area (655 m – 1010 m, red points). The blue dashed line indicates a possible trend that may link the shallow and deeper intervals.

To assess continuity between geomechanical properties in shallow (<100 m) and deeper (>650 m) intervals in the study area, the monitoring well data are plotted with data from an industry well (655m – 1010 m) (Figure 10B). While unit tops were not identified in the industry logs for depths shallower than 1000 m, the rock in this interval is likely part of the Cretaceous sequence. Due to the differences in depth (confining pressures), age, and importantly lithology (Paleocene vs Cretaceous sediments), and factors such as porosity and fracturing in the softer shallow sediments, the plot shows some lack of continuity between shallow and deep datasets.

Hydrogeophysical Logs

Fractures, matrix permeability, and stratigraphic heterogeneities (including cemented beds) create complex conditions for site-wide hydrogeological assessment. The rough and fractured conditions of the borehole walls further complicate the interpretation of discontinuities (potential groundwater flow pathways) within the greater rock mass. The acoustic televiewer identified numerous intervals with discontinuous openings – both bedding-parallel and higher angle joints. The hydrogeophysical logs help identify which structures facilitate water movement along and through each open, hydraulically cross-connected borehole. It should be noted that an open borehole provides a conduit for hydraulic connection that would not normally exist without this flow path.

A combined interpretation of the televiewer and video camera images, fluid temperature/conductivity, and flow meter logs provided:

- on-site guidance for the installation of screened intervals following the drilling;
- information on the direction of vertical fluid flow, informing the discharge or recharge setting of the boreholes;
- information on the temperature and conductivity of the borehole fluid, and where properties are changing due to fluid flow entering/exiting the well through transmissive fractures or the rock matrix;
- information on the presence and distribution of fractures transmitting fluid in the well; and
- insight into the local hydrostratigraphy, thereby inferring which layers are acting as aquitards and creating hydraulic gradients.

Vertical Fluid Flow

Natural vertical fluid movement was measured in all six boreholes where the heat pulse flow meter was deployed (Table 8). All the boreholes recorded down flow, except for MW-10-A where up flow was recorded. Although HPFM data were not collected in MW-6-D or MW-9-A, down flow was inferred in these two boreholes from interpretations of the video log and fluid log responses. These results indicate primarily a recharge area, with the exception of borehole MW-10-A located very close to a stream where discharging groundwater was observed. These results are in agreement with the findings of Smerdon et al. (2016) immediately south of the study area, and with the regional trends observed further to the south by Grasby et al. (2008), both who note largely downward flow across much of the Paskapoo.

Table 8 – Flow direction and flow rates measured with a heat pulse flowmeter.

Borehole	Flow Direction	Flow Range (L/min)
MW-1-C	Down	0.03 – 0.10
MW-3-B	Down	0.3 - >> 4
MW-3-C	Down	0.17 – 0.50
MW-3-D	Down	0.04 - >> 4 (one up flow of 0.1)
MW-8-C	Down	0.31 single measurement, electrical issue with flow meter
MW-10-A	Up	0.08 – 0.16

Fluid Properties

A fluid temperature/conductivity tool was the first instrument run in the holes after drilling was completed. In three of the eight wells (MW-3C, -8-C, -9-A), fluid logs were collected a second time at the start of a new shift (2:30, 18:45, and 14:00 hours after the first run, respectively), allowing for greater

thermal equilibration and examination of the contrast between fluid log runs (Figure 11). This provided insight into the movement of fluid in the well, as groundwater temperatures affected by drilling activities equilibrate over time. In intervals of higher vertical hydraulic gradients (greater flows), there was a rapid stabilization of water temperatures and conductivities, while in intervals of reduced vertical gradients (lower flows) in the base of the wells, temperatures and conductivities equilibrated at different rates (see arrows). These repeat logs helped to identify discontinuities with fluid movement, and supported the selection of heat pulse flowmeter test intervals.

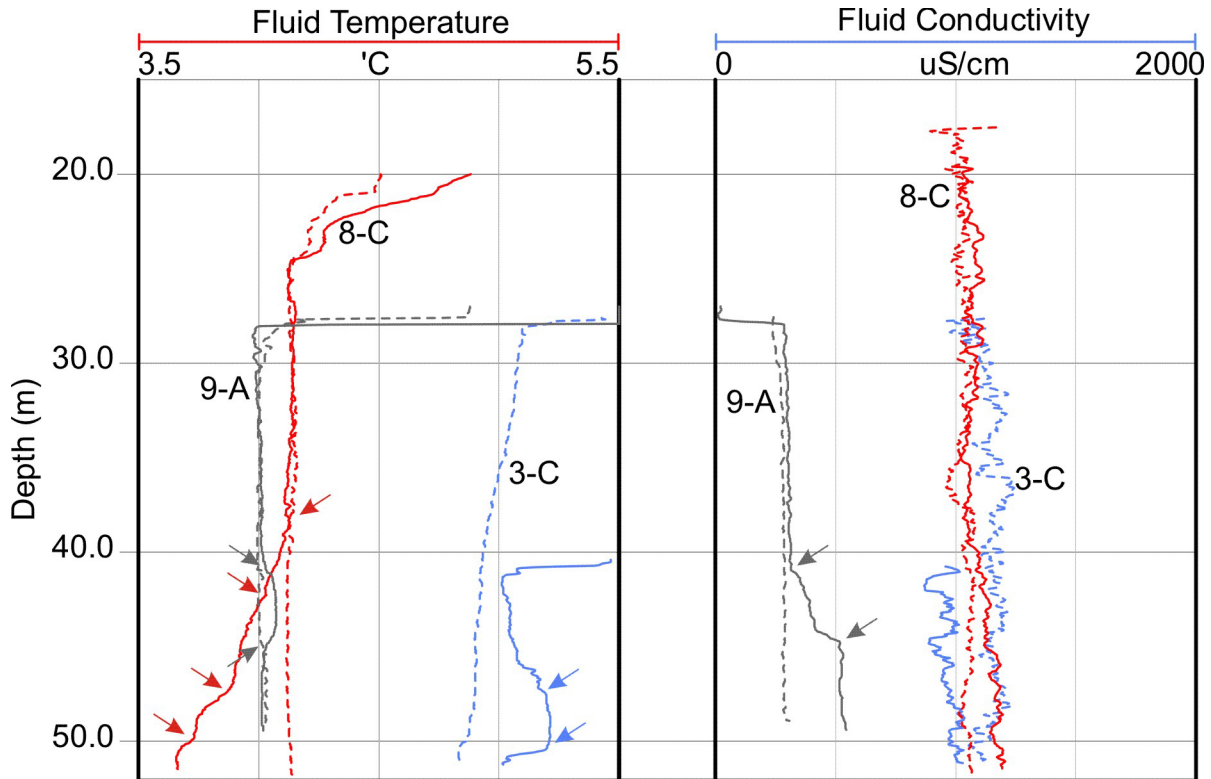


Figure 11 – Repeat fluid temperature and conductivity after drilling (solid line) versus several hours after the first log (dashed line). The more abrupt changes in the early log, still influenced by drilling activities, identified intervals where fluid exchange in the well varied; in the later log, these effects are subdued as fluid conditions equilibrate.

The ranges of fluid properties in the wells are shown in Figure 12 where the most stabilized logs in each well are plotted (selecting the dotted lines in Figure 11). In the down flowing wells, the temperature ranged from 4.0 – 5.0°C (once below the top of the water column which is influenced by air temperatures). This is a relatively narrow range and suggests the influence of vertical flow. The fluid temperature in the up flowing well was nearly a degree colder (3.25 – 3.75°C). These low groundwater temperatures may reflect the mean annual air temperature in the region (approximately 3°C), but local variation may reflect the rate of recharge from well to well.

Fluid conductivities ranged from 240 – 1900 µS/cm (uncorrected for temperature) without a clear distinction between up and down flow trends. This range is compared to conductivities measured on groundwater samples collected following the screen installations after wells were developed for 2⁺ hours. Conductivities of samples using a hand-held meter ranged between 470 to 1470 µS/cm (when corrected to 25°C). Adjusting these to approximate borehole temperatures of 4°C gives a range of

approximately 270 to 850 $\mu\text{S}/\text{cm}$. The conductivity log plot in Figure 12 indicates that there is close agreement between groundwater samples and log measurements in the low end of the range, but suggests some influence from recent drilling activities in logs with more elevated conductivities. The lowest log conductivities are measured in MW-9-A, where very little till exists at surface (3.4 m). Given its high elevation and degree of fracturing, this borehole may be influenced by more rapid recharge than at the other boreholes. In contrast, more elevated conductivities ($>1300 \mu\text{S}/\text{cm}$) in wells MW-6-D and MW-3-D are found in intervals containing shaly sediments (shaly sandstone and shale, respectively) which are likely influencing borehole fluid conductivity with logging carried out only hours after drilling.

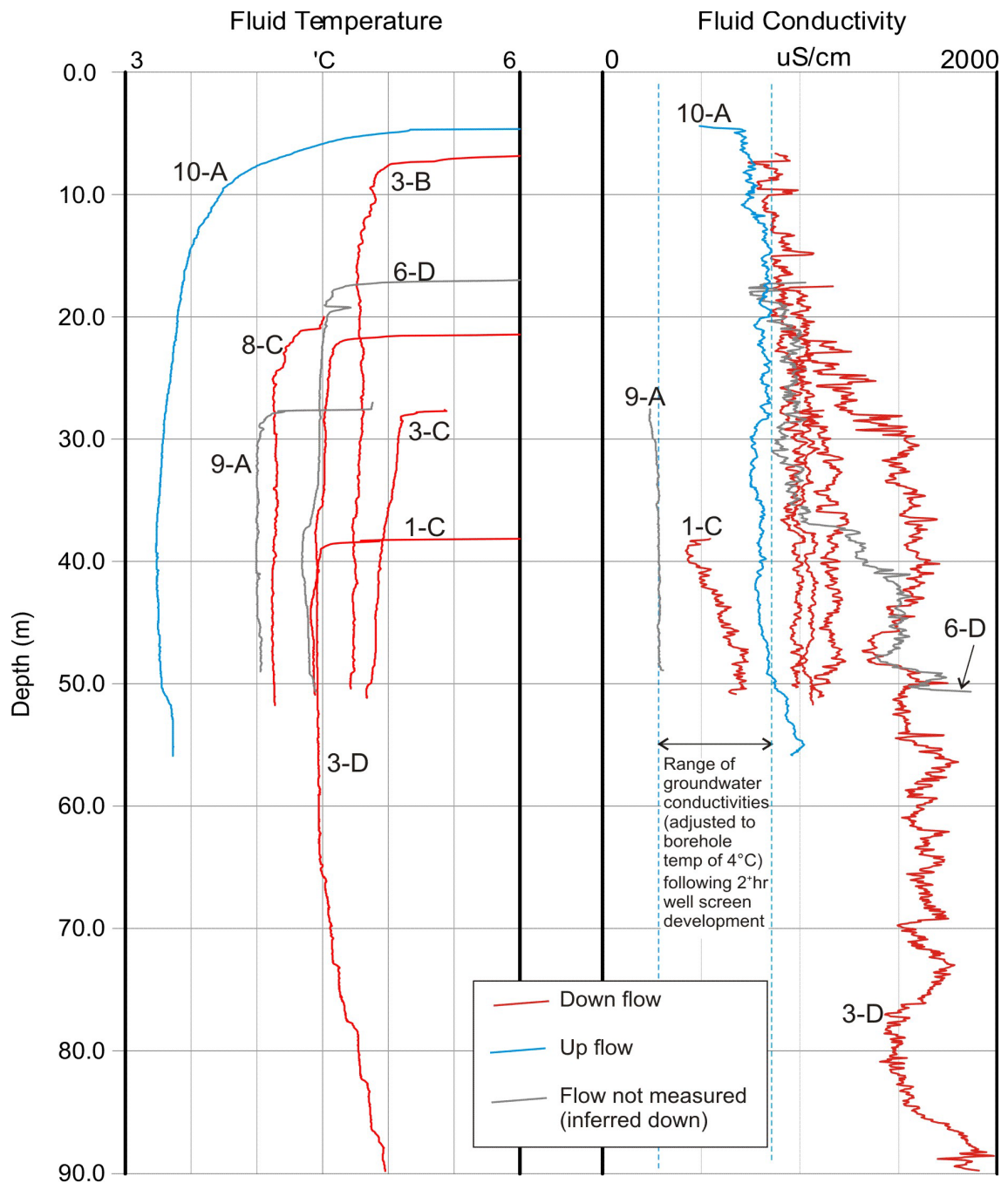


Figure 12 – Fluid temperature and conductivity logs plotted relative to depth, colour coded by flow direction. Down flow inferred for wells MW-6-D and -9-A.

Fluid Pathways

The presence of vertical flow is created in open boreholes by cross-connection of fractures with different hydraulic heads. Fractures are interpreted as transmitting fluid (“flowing”) when a change in vertical flow rate is measured above/below a continuously open fracture, and/or if changes in fluid temperature/conductivity are observed at an enlargement in the borehole wall identified by the ATV image/caliper log (e.g. conditions met in Figure 13A). In total, 38 flowing fractures were interpreted with these criteria. This number is considered to be a conservative estimate, given that (1) open fractures can be flow paths even if a change in the vertical gradient is not measured across a fracture; (2) fluid can be moving in or out of a fracture and not creating fluid temperature or conductivity anomalies; and (3) flow meter data were not available in three of the eight wells. Despite these uncertainties, the data indicate that fluid is moving throughout the rock mass along open, predominantly bedding-parallel fractures from top of rock to depths exceeding 50 m, although only one well extended to 90 m (Figure 14). Grasby et al. (2008) note that fracture surfaces observed in core can show oxidation compared to the surrounding rock mass. Iron staining appears to be present on some fracture surfaces in the video logs (Figure 8C), providing further evidence that weathering is occurring along bedding planes and fractures are providing pathways for flow.

The relatively low number of open fractures (typically 0.5 to 1.0 per 2 m interval) suggests that ground water is also moving through the sandstone matrix with a fracture flow system overprint. Grasby et al. (2008) note that in low fracture density rock (< 2 frac/m) with thicker beds (>50 cm), porous flow likely dominates. Many examples in the Fox Creek boreholes exist where changes in flow are observed across intervals without distinct, continuous open fracture(s). This does not exclude the presence of flow along small bedding planes or discontinuous features not resolved within the borehole wall, but also suggests the presence of matrix flow through the more porous sandstone matrix. While no-flows (<0.03 L/min) are measured in the bottom of five of the six boreholes flow metered, in MW-3-B, down-flowing groundwater is measured just above the base of the borehole (0.3 – 0.50 L/min), indicating downward gradients can extend beyond 50 m (Figure 13B). Additionally, the relatively flat temperature gradients seen in the three boreholes where logs were collected many hours after the drilling suggest vertical water movement (Figure 11). In boreholes MW-3B and -3C, down flowing fluid moves past a cemented sandstone bed and is reabsorbed into the more porous sandstone matrix intersected at the base of the wells (42 – 50 m and 44.7 – 50 m, respectively). This scenario of downward flowing groundwater through matrix and fracture pathways supports the findings from Rivard et al. (2022) that the groundwater throughout the study area is predominantly of the CaHCO₃ type, corresponding to relatively young, downward-recharging water.

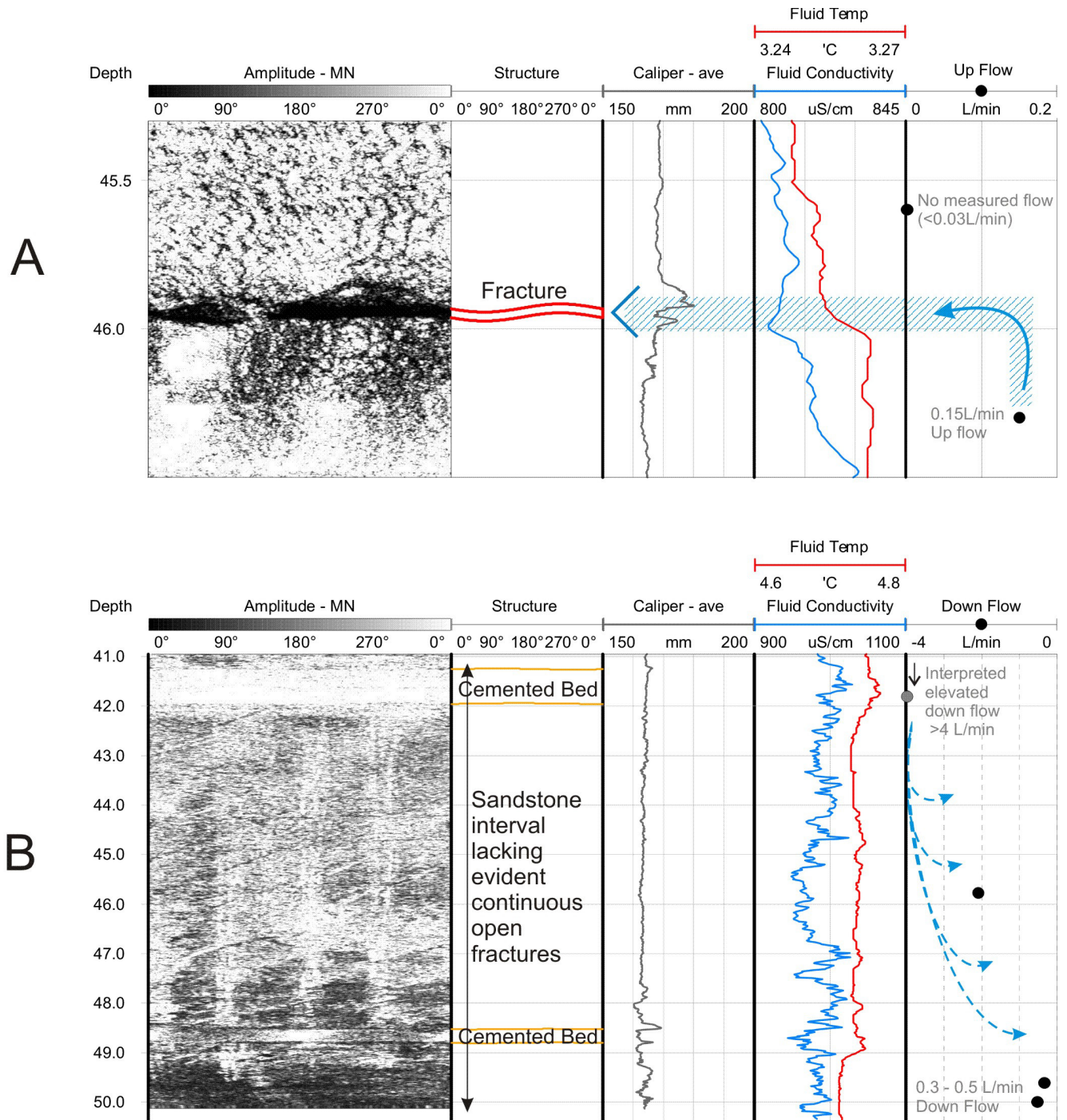


Figure 13 – Vertical flow in boreholes enters and exits the rock mass through both (A) discrete open fractures (e.g. MW-10-A), and (B) permeable zones in rock matrix (e.g. MW-3-B).

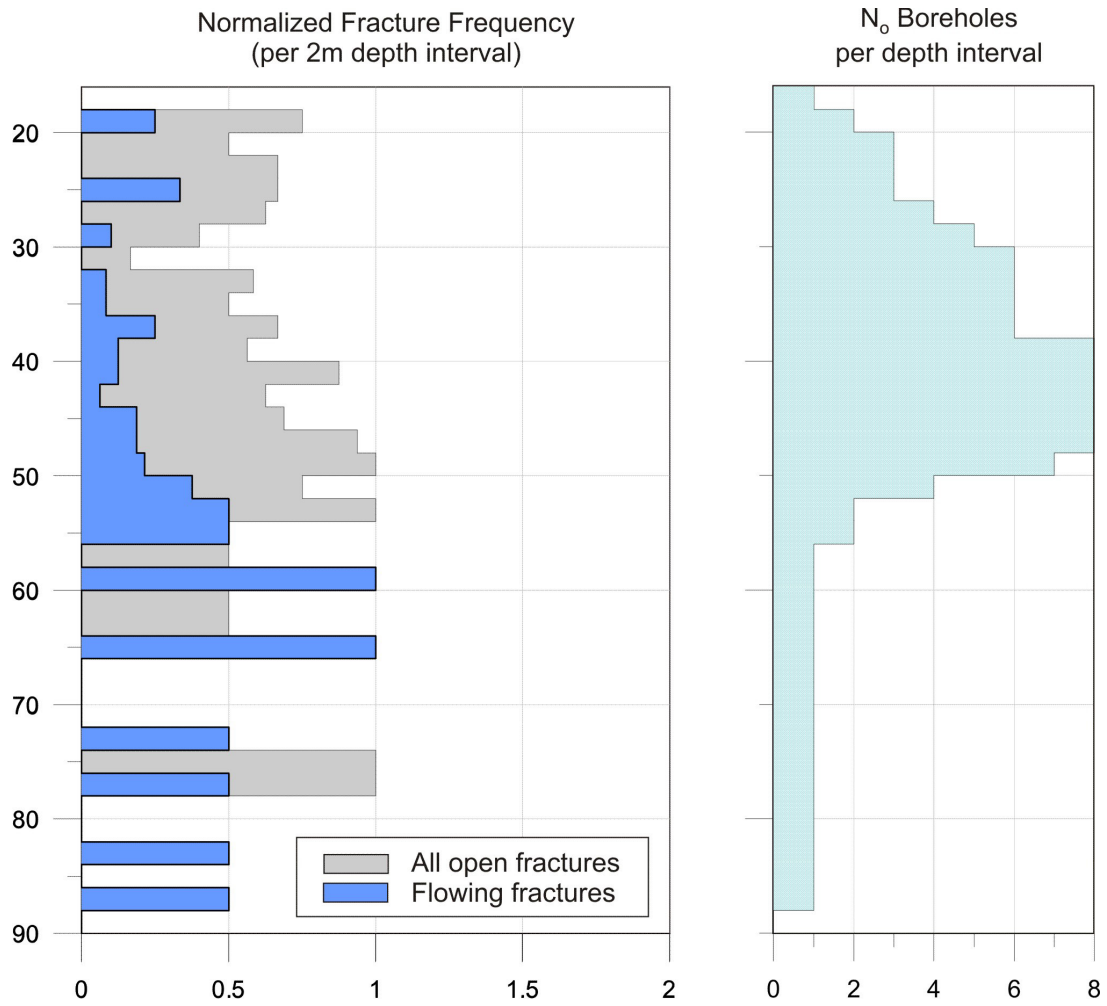


Figure 14 – Interpreted fracture frequency per 2 m depth interval. Frequency is normalized by number (N_o) of boreholes with televiewer logs in each depth interval, shown in right panel.

Summary

The main findings of the study are:

- Lithological logs (natural gamma, density, resistivity, velocity, and acoustic amplitude logs):
 - indicated variability across the shallow bedrock that could help refine stratigraphic logs from cuttings descriptions, and
 - identified the presence of 25 high velocity/density/resistivity beds (0.50 ± 0.25 m in thickness) predominantly found in the sandstone (n=20).
- The mean density of all rock types logged is 2.39 ± 0.10 g/cm³ with a mean V_p of 2270 ± 335 m/s and V_s of 1240 ± 50 m/s. Agreement between core and log densities is very high ($R^2=0.99$) for eight core samples.
- These V_p and density results are within ranges measured during a previous study carried out near Fox Creek. However, these velocities are relatively low, and borehole wall conditions contribute to difficulties in the interpretation of the data, particularly V_s. The non-standard results of the semblance processing technique for V_s interpretation may be indicative of DTS times merging with tube waves travelling along the borehole walls. The GSC followed up with core testing in two boreholes drilled adjacent to logged holes. Core results were varied but velocity ratios (Poisson's ratios) between V_p and V_s were in range of those calculated from the downhole logs.
- The two most frequently described rock types (identified from cuttings during the drilling) are sandstone and shale. Once the high velocity beds are removed from the datasets, mean sandstone density is 2.35 ± 0.08 g/cm³ and V_p is 2200 ± 325 m/s. Mean shale density is 2.42 ± 0.08 g/cm³ and V_p is 2255 ± 205 m/s. The lower densities/velocities of the sandstones are interpreted to reflect higher porosities, which can provide preferential pathways for matrix flow.
- The high velocity/density beds have a mean density of 2.53 ± 0.11 g/cm³ (with a maximum of 2.71 g/cm³) and a mean V_p of 2910 ± 520 m/s (with a maximum of 4675 m/s). These intervals are interpreted as cemented and may represent barriers to vertical flow. However, the lateral extent, or presence of vertical fracturing in these layers, is unknown.
- Dynamic elastic moduli (Poisson's ratio and Young's modulus) were calculated for the shallow bedrock after intervals affected by highly fractured rock walls were removed. Mean Poisson's Ratio (ν) is interpreted as 0.27 ± 0.06 but with a wide range of values (0.10 – 0.44) likely reflecting both the range in sediment conditions (i.e. the heterogeneity of the Paskapoo Formation) and the drilling technique causing wall roughness in the poorly consolidated rock of the Paskapoo Formation affecting V_s value interpretation. The mean Young's Modulus (E) is 9.50 ± 1.28 GPa, which is relatively low and reflects the softness of the rock, the shallow setting, and the low interpreted values of V_s. A cluster of points outside of the general data trend reflects the higher density/velocity of the cemented beds.
- Downward flowing groundwater was interpreted in all the wells but one, indicating that recharge conditions are prevalent in the study area; one up-flowing well indicates discharge conditions close to a stream.
- Downhole fluid temperatures of recharging groundwater range between 4 and 5°C, likely reflecting the mean annual air temperature of the study area (approximately 3°), but locally variable depending on season and recharge rates. The discharging borehole had water temperatures one degree cooler, ranging from 3.25 – 3.75°C.

- The majority of open discontinuities (fractures) observed in the borehole walls (n=145) were bedding-parallel (n=115). Thirty-eight of these open fractures (33%) were interpreted as transmitting fluid into/out of the well due to cross-connection between fractures with different hydraulic heads (although all open fractures can be flow paths). Of these 38 features, only six high angle joints were interpreted as transmitting fluid under ambient conditions. This suggests the majority of flow through discontinuities was along bedding partings.
- Fluid pathways are interpreted to be both along discontinuous fractures and through the sandstone matrix. A relatively low number of open fractures (typically 0.5 to 1.0 per 2 m interval) suggests that ground water is both moving through the porous sandstone matrix and through the fracture system.
- The results of the downhole logs provide inputs for the shallow groundwater flow models.

Acknowledgements

With thanks to the field team of Andrew Brennan, Tyler Corriveau, and Shawn Collins (Wireline Services Group) who collected the geophysical data under challenging field conditions. Thanks also to Amit Sharma and Rob Wenzel (Matrix Solutions) and to Nick Skinner (Full Metal Drilling) for field support and well drilling. Thanks to Christine Rivard and Vincent Tremblay (Geological Survey of Canada) for project leadership, co-ordination, and data management. The author gratefully acknowledges reviews of this report by Drs. Christine Rivard, Peeter Pehme, and Elena Konstantinovskaya.

Funding for this work was provided through the Environmental Geoscience Program and the Groundwater Geoscience Programs of the Geological Survey of Canada, Natural Resources Canada.

References

- Crow, H.L., Cartwright, T.J., and Ladevèze, P. 2017. Downhole geophysical data collected in 10 boreholes near Sussex, New Brunswick; Geological Survey of Canada, Open File 8310, 1 .zip file. <https://doi.org/10.4095/306173>
- Crow, H.L., Brewer, K.D., Cartwright, T.J., Gaines, S., Heagle, D., Pugin, A.J.-M., and Russell H.A.J. 2021. New core and downhole geophysical data sets from the Bells Corners Borehole Calibration Facility, Ottawa, Ontario; Geological Survey of Canada, Open File 8811, 1 .zip file, <https://doi.org/10.4095/328837>
- Gercek, H. 2006. Poisson's ratio values for rocks (Review), *International Journal of Rock Mechanics & Mining Sciences*, 44, p.1-13.
- Grasby, S.E., Chen, Z., Hamblin, A.P., Wozniak, P.R.J., Sweet, A.R. 2008. Regional characterization of the Paskapoo bedrock aquifer system, southern Alberta. *Canadian Journal of Earth Science*, 45, p.1501-1516.
- Guarin Martinez. L.I. 2022. Characterization and numerical modeling of the bedrock aquifer in the Fox Creek area, Alberta, M.Sc. thesis, Institut national de la recherche scientifique – Centre Eau Terre Environnement (INRS-ETE), 122 pages.
- Lavoie, D., Tremblay, V., and Rivard, C., 2023. Sandstone composition and diagenesis of the Paskapoo Formation and their significance for shallow groundwater aquifer in the Fox Creek area, west-central Alberta. Geological Survey of Canada, Open File 8982, 92 pages. <https://doi.org/10.4095/331923>
- Paillet, F.L., Cheng CH, 1991. *Acoustic waves in boreholes*, CRC Press Inc., Florida, 264p.
- Rivard, C., Paniconi C., Bordeleau, G., Crow, H., Meneses-Vega, B.J., Guarin-Martinez, L.I., Kononovs, D., Alessi, D., Degenhardt, S.D., 2022. Fox Creek project on cumulative effects: an update from the groundwater perspective, in proceedings of GAC-MAC-IAH, Halifax, Nova Scotia, May 15-18, 2022.
- Saxena, V., Krief, M., and Adam, V., 2018. *Handbook of borehole acoustics and rock physics for reservoir characterization*. Elsevier, 455 pages.
- Smerdon, B.D., Atkinson, L.A., Hartman, G.M.D., Playter, T.L., Andriashek, L.D. 2016. Field evidence of nested groundwater flow along the Little Smoky River, west-central Alberta; Alberta Energy Regulator, AER/AGS Open File Report 2016-02, 34p.
- Wireline Services Group (WSG), 2021. Calibration report for geophysical data collected at Fox Creek, Alberta, Canada; Multi-parameter geophysical logging of shallow monitoring wells; Internal report, 13p.